Supplementary Information: Sparse Cyclic Excitations Explain the Low Ionic Conductivity of Stoichiometric $Li_7La_3Zr_2O_{12}$

Functional form of the DIPPIM model

The DIPole Polarizable Ionic Model (DIPPIM) potential [1–3] has previously been used to study metal oxides [4–8], and fluoride systems [9, 10]. The potential is constructed from four components corresponding to the charge–charge, dispersion, overlap repulsion, and polarization interactions; each of which is described below. Terms indicated in red in Eqns. S2–S7 are parameterised for LLZO by fitting to *ab initio* forces, dipoles, and stress tensors, and are reported in Table S1.

Coulomb Interactions

Coulombic (charge–charge) interactions are described by

$$V^{\mathrm{qq}} = \sum_{i \leq j} \frac{q_i q_j}{r_{ij}}, \tag{S1}$$

where q_i is the formal charge on ion i.

Dispersion Interactions

Dispersion interactions include dipole–dipole and dipole–quadrupole terms:

$$V^{\mathrm{disp}} = -\sum_{i \leq j} [\frac{f_6^{ij}(r^{ij}) C_6^{ij}}{r_{ij}^6} + \frac{f_8^{ij}(r^{ij}) C_8^{ij}}{r_{ij}^8}]. \tag{S2}$$

C_6^{ij} and C_8^{ij} are the dipole–dipole and dipole–quadrupole dispersion coefficients, respectively. The f_n^{ij} are Tang-Toennies damping functions [11, 12] which describe the short-range penetration correction to the asymptotic dispersion term:

$$f_n^{ij}(r_{ij}) = 1 - e^{b_n^{ij} r_{ij}} \sum_{k=0}^{n} \frac{(b_n^{ij} r_{ij})^k}{k!}. \tag{S3}$$

Overlap Repulsion Interation

The short range repulsive term is approximately exponential in the region of physical interionic separations. The full expression used also includes a Gaussian function which acts as a steep repulsive wall and accounts for the repulsion between core electronic states. This extra term is particularly beneficial in systems with highly polarizable ions (e.g. oxygen) where it helps avoid numerical instabilities in the dipoles that can occur at very small (unphysical) anion–cation separations [13].

$$V^{\mathrm{rep}} = \sum_{i \leq j} \frac{A^{ij} e^{-a^{ij} r_{ij}}}{r_{ij}} + \sum_{i \leq j} B^{ij} e^{-b^{ij} r_{ij}^2}. \tag{S4}$$

Dipolar Interaction

The polarization part of the DIPPIM potential incorporates dipolar effects:

$$V^{\mathrm{pol}} = \sum_{i,j} \left(q_i \mu_{j,\alpha} f_4^{ij}(r_{ij}) - q_j \mu_{i,\alpha} f_4^{ji}(r_{ij}) \right) T_\alpha^{(1)}(\mathbf{r}_{ij}) - \sum_{i,j} \mu_{i,\alpha} \mu_{j,\beta} T_{\alpha\beta}^{(2)}(\mathbf{r}_{ij}) + \sum_i \frac{1}{2\alpha_i} \mid \boldsymbol{\mu}_i \mid^2 . \tag{S5}$$

Here α_i is the polarizability of ion i, $\boldsymbol{\mu}_i$ are the dipoles and $\mathbf{T}^{(1)}$, $\mathbf{T}^{(2)}$ are the charge–dipole and dipole–dipole interaction tensors:

$$T_\alpha^{(1)}(\mathbf{r}) = -r_\alpha / r^3 \qquad T_{\alpha\beta}^{(2)}(\mathbf{r}) = (3 r_\alpha r_\beta - r^2 \delta_{\alpha\beta}) / r^5 \tag{S6}$$

The short-range induction effects on the dipoles are taken into account by the Tang-Toennies damping functions (f_4^{ij}) similar to those used to damp the dispersion interactions (Equation S7) where b^{ij} determines the range at which the overlap of the charge densities affects the induced dipoles. The damping of these induction effects requires an additional pre-exponential parameter, c^{ij}, which determines the strength of the ion response to this effect [11, 12],

$$f_n^{ij}(r_{ij}) = 1 - c^{ij} e^{-b^{ij} r_{ij}} \sum_{k=0}^{n} \frac{(b^{ij} r_{ij})^k}{k!}. \tag{S7}$$

The instantaneous values of the dipole moments are obtained by minimization of this expression with respect to the dipoles of all ions at each MD timestep. This ensures that we regain the condition that the dipole induced by an electrical field $\mathbf{E}$ is $\alpha\mathbf{E}$, and that the dipole values are mutually consistent.

Interatomic Potential Parameter Fitting

A benefit of the IP parameterization approach presented here, is that the parameters are derived entirely from *ab initio* data, with no direct input of experimentally data. The quality of any parameter set is determined by the agreement between the DFT training set

and the equiavlent DIPPIM data, calculated for a given set of potential parameters. Our fitting was performed against the following training set of configurations modelled using DFT: 3 stoichiometric LLZO cells (each with 192 atoms), where two had tetragonal cell symmetry, and the other had cubic cell symmetry. These were given initial lithium distributions by randomly arranging the lithiums over the tetrahedral and octahedral sites to achieve an occupancy ratio equal to that of Xu *et al.* [14], i.e. 43% of the Li ions in tetrahedral positions and the remainder in the octahedral positions.; Two Al-doped LLZO cells with compositions $Li_{4.0}Al_{1.0}La_3Zr_2O_{12}$ and $Li_{4.75}Al_{0.75}La_3Zr_2O_{12}$.; One Nb-doped LLZO cell and One Ta-doped LLZO cell, both with compositions $Li_{6.0}La_3ZrMO_{12}$, one cell each with compositions $Li_5La_3Nb_2O_{12}$ and $Li_5La_3Ta_2O_{12}$, and two $2\times2\times2$ supercells of $LiAlO_2$. Dopant atoms were randomly placed in the LLZO cells, with Al occupying only tetragonal Li sites, and Nb or Zr occupying Zr sites. Fitting was performed against all configurations in this training set simultaneously.

Each configuration included in the fit was prepared using *ab initio* MD simulations at a temperature of 2000 K using the PBE functional[15] with a 300 eV plain wave cut-off, k-point sampling at the gamma point only and a timestep of 1 fs. All *ab initio* simulations were performed using the VASP code [16, 17]. The cells were equilibrated for 50 ps to ensure that the forces on most ions were greater than 1 eV $Å^{-1}$. Following this high temperature equilibrations, static h-DFT (using the HSE06 functional [18, 19]) calculations with a plane wave cut-off of 500 eV were performed to obtain reliable forces and stress tensors. The resulting wavefunctions were post-processed using the `wannier90` library [20] and the Wannier centres were used to calculate the dipole moments on each ion [21]. The final χ^2 values were 0.130, 0.206 and 0.160 for the dipoles, forces and stress tensors, respectively. Our fitted parameter set is provided in Table S1.

The dipole polarizabilities for La^{3+}, Zr^{4+} and O^{2-} were obtained from previous work [22], while those for Nb^{5+} and Ta^{5+} were derived as part of the fit. Dispersion terms were derived from these polarizabilities via the Slater-Kirkwood equation [22, 23].

The DIPPIM forces, dipoles, and stress tensors obtained from this procedure are shown in Fig. S1 for one LLZO configuration, for comparison with the corresponding training set h-DFT values. The close agreement between DIPPIM values and the original h-DFT training set indicates the fitted potential offers an accuracy comparable to the reference h-DFT calculations, at a computational cost several orders of magnitude lower.

The quality of the fitted potential can also be evaluated by comparing forces and dipoles for the DIPPIM model against those calculated use h-DFT for a LLZO configuration *not in the initial training set*. We have done this

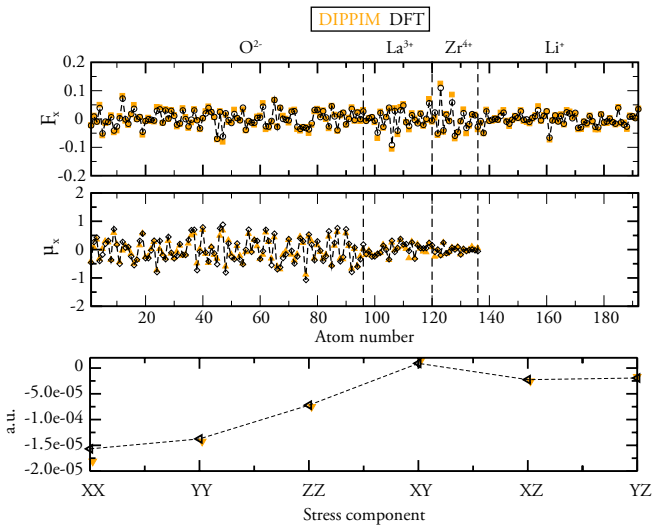

FIG. S1. DIPPIM (filled orange symbols) and h-DFT (open black symbols) calculated forces (top), dipole moments (middle) and stress tensors (bottom) in atomic units.

for a configuration generated by a short AIMD simulation at 600 K. Figure S2 shows scatter plots of the corresponding forces (top) and dipoles (bottom) for both HSE (abscissa) and DIPPIM (ordinate). The strong correspondence supports the accuracy of the DIPPIM model. Interestingly, this comparison reveals that the DIPPIM model underestimates dipoles at high values, which may be due to our model only considering the linear first-order polarisation term, and suggests an even better parameterisation would be possible for a potential model that incorporated hyperpolarisabilities.

Simulation Details

All MD simulations on the lithium garnet $Li_7La_3Zr_2O_{12}$, were performed using $2\times2\times2$ supercells with 1536 atoms that were generated from the cells used to perform the potential parameterization (See below). The supercells were initially equilibrated at a temperature of 280 K for 10 ps; the temperature was then scaled up to 1000 K at a rate of 1 K ps^{-1} to study the changes in lattice constant as a function of temperature. All the equilibration simulations were performed at constant temperature and pressure (NPT ensemble), as described by Martyna *et al.* [24] using a time step of 1 fs. The Coulombic interactions were summed using Ewald summations [25]. The short-range part of the potential was truncated at 12.96 Å.

TABLE S1. Parameters for the DIPPIM potential. All values are in atomic units. The parameters $b_D^{O^{2-},\square}$ and $b_D^{\square,O^{2-}}$ were given the same value. $\square$ is a placeholder for the identity of the ionic species specified in the first column.

Interaction	A^{ij}	a^{ij}	B^{ij}	b^{ij}	C_6^{ij}	C_8^{ij}	b_6^{ij}	b_8^{ij}
O^{2-} – O^{2-}	0.00	5.00	50000	0.95	83.0	1240.0	1.30	1.70
Zr^{4+} – O^{2-}	70.58	1.21	50000	1.75	21.0	271.0	1.62	2.10
La^{3+} – O^{2-}	103.48	1.27	50000	1.30	57.0	731.0	1.46	1.88
Li^{1+} – O^{2-}	20.29	1.39	50000	2.06	0.00	0.00	–	–
Al^{3+} – O^{2-}	40.04	1.26	50000	2.10	0.00	0.00	–	–
Nb^{5+} – O^{2-}	58.15	1.12	50000	1.80	17.6	224.8	1.86	2.42
Ta^{5+} – O^{2-}	58.14	1.12	50000	1.80	17.4	222.3	1.86	2.42

Ion	α	$b_D^{O^{2-}-\square}$	$c_D^{O^{2-}-\square}$	$c_D^{\square-O^{2-}}$
O^{2-}	13.97	2.11	2.86	–
Zr^{4+}	2.38	1.74	1.60	-0.75
La^{3+}	7.51	1.72	2.09	0.03
Li^{1+}	–	1.82	1.42	–
Al^{3+}	–	1.80	1.41	–
Nb^{5+}	1.97	1.80	1.46	-0.91
Ta^{5+}	1.88	1.79	1.57	-0.55

Validation of the Interatomic Potential

The quality of the DIPPIM model was assessed from its ability to accurately predict the structure and dynamics of LLZO, by performing comparisons with available experimental data (for the structure) and DFT-based MD results (for the lithium diffusion).

TABLE S2. Experimental and calculated lattice constants for t-LLZO at 300 K.

Source		a (Å)	c (Å)
XRD	Rangasamy *et al.* [26]	13.068	12.702
DFT (PBE functional)	Meier *et al.* [27]	13.208	12.659
DIPPIM	this work	13.180	12.849

The room temperature lattice constants obtained with DIPPIM are presented in Table S2 along with experimental and DFT literature values. The room temperature lattice parameters from the DIPPIM model are approximately 1% larger than experimental values, as would be expected due to the h-DFT functional used lacking dispersion interactions and also slightly overestimating the volume. LLZO undergoes a phase transition from a tetragonal to cubic lattice at temperatures above 600 K. Experimental transition temperatures depend strongly on the incorporation of Al during sample preparation, and on exposure to air [28, 33]. The DIPPIM potential predicts a tetragonal (t-LLZO) crystal structure below 620 K and a cubic (c-LLZO) structure above 620 K (Fig. S3 (a)). This agrees with the experimental value of 623 K of Kuhn *et al.* , and with the value of 600 K from the DFT-based MD simulations of Bernstein *et al.* [34].

The calculated DIPPIM Li–Li partial radial distribution functions, $g(r)$, for t-LLZO at 300 K are presented in Fig. S3 (b) (green) along with those obtained by neutron scattering experiments (black) and the shell model from the work of Klenk and Lai [29]. The $g(r)$ from MD simulations using the soft bond-valence model of Adams and Rao [30] is shown in blue. The DIPPIM shows an excellent agreement with the experimental structure over the whole range of distances. Further confirmation that the DIPPIM model predicts the correct structure for LLZO was obtained by comparing the predicted fractional occupancies of the tetrahedral and octahedral sites as a function of temperature in t-LLZO with those obtained experimentally (Fig. S3 (d)). The experimental occupancy of the tetrahedral sites at room temperature obtained from NMR [28] is 0.14, in excellent agreement with our simulated value of 0.15.

We have also compared the lithium diffusion coefficients calculated using the DIPPIM MD simulations, to those obtained from *ab initio* MD by Miara *et al.* [31] and Jalem *et al.* [32] (Fig. S3 (d)). The values span a range of 400–1000 K because no diffusion was observed at 300 K despite the long simulation time (87 ns). Both high-temperature c-LLZO (low activation energy) and low-temperature t-LLZO (high activation energy) regions are present in the DIPPIM data. The *slope* of the DIPPIM calculated diffusion coefficients, which corresponds to the effective activation energy for diffusion, is very similar to those from the previous *ab initio* MD simulations in the c-LLZO region, and shows the increase in activation energy below 600 K where the t-LLZO phase is stabilised. The absolute diffusion coefficients are predicted to be larger than those from previous *ab initio* MD calculations. This is, in part, due to our calculations using cells equilibrated at each temperature under NPT conditions (giving zero-pressure volumes), while the simulations of Miara *et al.* and Jalem *et al.* were performed at smaller 0 K DFT calculated cell volumes. For a direct comparison, we have also calculated DIPPIM diffusion coefficients for c-LLZO in cells constrained at the DIPPIM 0 K volume, and at

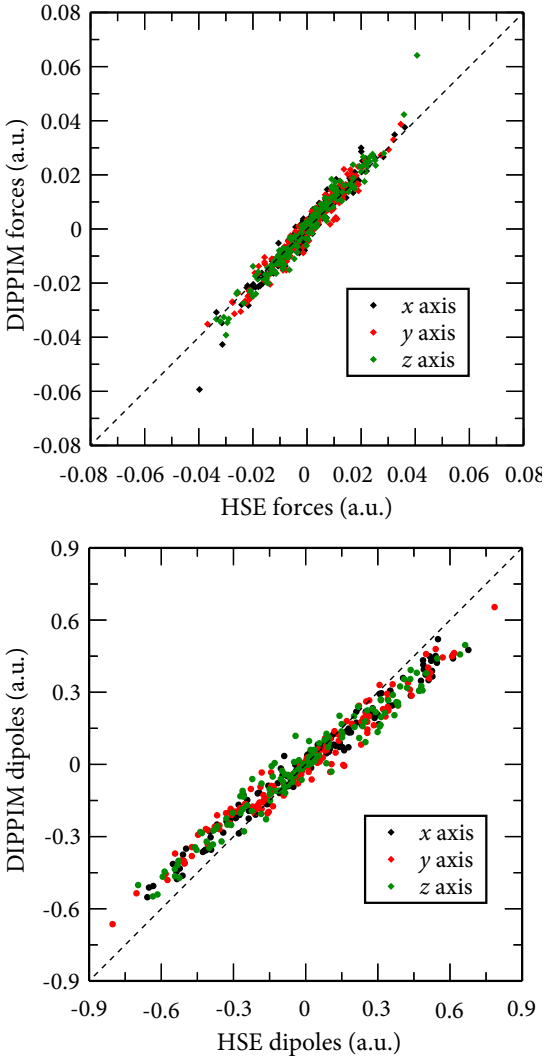

FIG. S2. Scatter plots of the forces (top) and dipoles (bottom) obtained for a representative configuration of c-LLZO at 600 K. In The x, y and z components of these quantities are represented in black, red and green, respectively. All values are in atomic units (a.u.).

the even smaller PBEsol 0 K volume used by Jalem *et al.* Smaller simulation cell volumes give decreased diffusion coefficients, following the effects of (negative) strain seen in other ionic conductors [35, 36], and bring the DIPPIM diffusion conductivities into much better agreement with previously calculated DFT (PBE / PBEsol) data. We also performed simulations on LLZO at high temperature, while constraining the tetragonal symmetry (DIPPIM t_{iso}) and obtained an activation energy of 0.47 eV, which is in good agreement with the value reported by Miara *et al.* for the same system, 0.43 eV. Nonetheless, exact agreement between the DIPPIM data and previous *ab initio* MD studies should not be expected for a number of reasons. Firstly, we have used a different DFT functional to the studies of Miara *et al.* and Jalem *et al.* Secondly, the DIPPIM potential, while physically motivated, still represents a model simplification of the true interatomic forces. A more sophisticated potential that included terms describing non-linear polarisation effects [37], or the dependence of oxygen short-ranged repulsion on local coordination environment [38] would be expected to give an even better *quantitative* description of experimental behaviour, albeit at an increased computational cost.

Extended excitation event

Fig. S4 shows a schematic of an example extended excitation event in t-LLZO at 300 K, which completes by meeting with itself after passing through the periodic boundaries of the cell.

[1] S. T. Norberg, I. Ahmed, S. Hull, D. Marrocchelli, and P. A. Madden, J. Phys.: Condens. Matter **21**, 215401 (2009).
[2] P. A. Madden, R. Heaton, A. Aguado, and S. Jahn, J. Mol. Struct.: THEOCHEM **771**, 9 (2006).
[3] M. J. Castiglione, M. Wilson, and P. A. Madden, J. Phys.: Condens. Matter **11**, 9009 (1999).
[4] D. Marrocchelli, P. A. Madden, S. T. Norberg, and S. Hull, J. Phys.: Condens. Matter **21**, 405403 (2009).
[5] M. Burbano, D. Marrocchelli, B. Yildiz, H. L. Tuller, S. T. Norberg, S. Hull, P. A. Madden, and G. W. Watson, J. Phys.: Condens. Matter **23**, 255402 (2011).
[6] M. Burbano, S. T. Norberg, S. Hull, S. G. Eriksson, D. Marrocchelli, P. A. Madden, and G. W. Watson, Chem. Mater. **24**, 222 (2012).
[7] D. Marrocchelli, M. Salanne, and P. A. Madden, J. Phys.: Condens. Matter **22**, 152102 (2010).
[8] M. Wilson, S. Jahn, and P. A. Madden, J. Phys.: Condens. Matter **16**, S2795 (2004).
[9] R. Heaton, R. Brookes, P. Madden, M. Salanne, C. Simon, and P. Turq, J. Phys. Chem. B **110**, 11454 (2006).
[10] M. Salanne, C. Simon, P. Turq, and P. Madden, J. Fluor. Chem. **130**, 38 (2009).
[11] K. T. Tang and J. P. Toennies, J. Chem. Phys. **80**, 3726 (1984).
[12] K. T. Tang and J. P. Toennies, J. Chem. Phys. **118**, 4976 (2003).
[13] M. J. Castiglione, M. Wilson, and P. A. Madden, J. Phys.: Condens. Matter **11**, 9009 (1999).
[14] M. Xu, M. S. Park, J. M. Lee, T. Y. Kim, Y. S. Park, and E. Ma, Phys. Rev. B **85**, 052301 (2012).
[15] J. P. Perdew, K. Burke, and Y. Wang, Phys. Rev. B **54**, 16533 (1996).
[16] G. Kresse and J. Furthmüller, Phys. Rev. B **54**, 11169 (1996).
[17] G. Kresse and J. Furthmüller, Comp. Mater. Sci. **6**, 15 (1996).
[18] J. Heyd, G. E. Scuseria, and M. Ernzerhof, J. Chem. Phys. **118**, 8207 (2003).

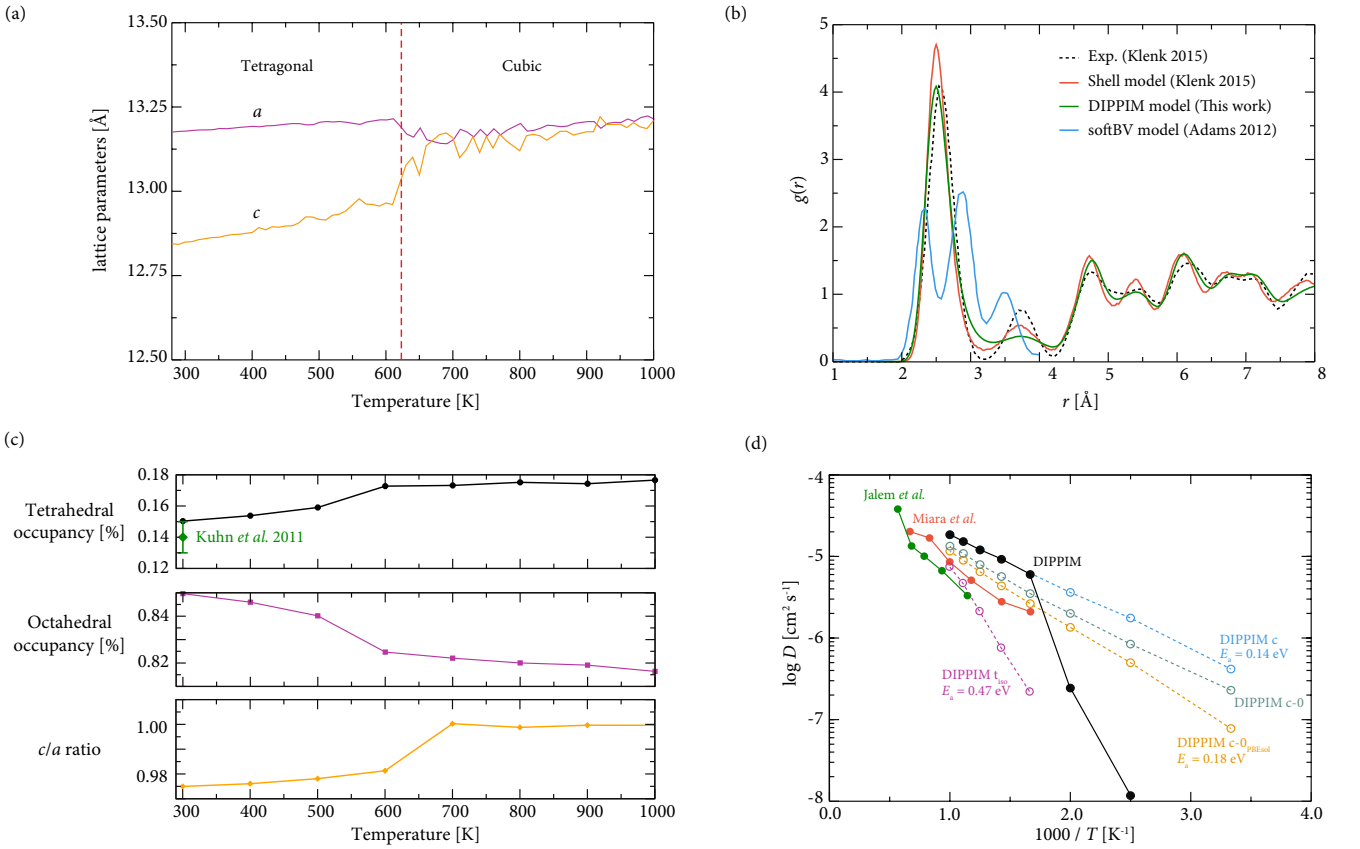

FIG. S3. (a) DIPPIM calculated lattice parameters for t-LLZO as a function of temperature. The *a* parameter is shown in magenta and the *c* parameter is shown in orange. The red dashed line marks the transition temperature of 623 K found experimentally by Kuhn *et al.* [28].
(b) A comparison of the Li–Li radial distribution function for t-LLZO from the parameterised DIPPIM model and from the works of Klenk and Lai [29] (Neutron scattering shown in black and shell model shown in red), and Adams and Rao [30] (soft Bond Valence force field shown in blue). DIPPIM results are shown in green.
(c) Occupancies of tetrahedral (top panel) and octahedral (middle panel) sites in pure LLZO as a function of temperature. The ratio of the *c*/*a* vectors in the same temperature range is presented in the bottom panel. The tetrahedral occupancy at room temperature found by Kuhn *et al.* [28] using NMR expriments is shown as a green diamond in the top panel.
(d) Diffusion coefficients for LLZO (black diamonds), corresponding to the MSDs presented in Fig. 2 of the main text. The *ab initio* MD values of Miara *et al.* [31] (red) and Jalem *et al.* [32] (green) are plotted for comparison. The DIPPIM data were calculated using cells equilibrated at each temperature under NPT conditions. We also show data for NPT equilibrated cells constrained to cubic symmetry (DIPPIM c), for cubic cells with the zero-temperature DIPPIM cell volume (DIPPIM c-0), and for cubic cells with the zero-temperature DFT cell volume (DIPPIM c-0_{PBEsol}) used by Jalem *et al.* .

[19] J. Paier, M. Marsman, K. Hummer, G. Kresse, I. C. Gerber, and J. G. Angyan, J. Chem. Phys. **124**, 154709 (2006).
[20] A. A. Mostofi, J. R. Yates, Y.-S. Lee, I. Souza, D. Vanderbilt, and N. Marzari, Comp. Phys. Commun. **178**, 685 (2008).
[21] L. Bernasconi, M. Wilson, P.A. Madden, Comp. Mater. Sci. **22**, 94 (2001).
[22] M. Burbano, S. Nadin, D. Marrocchelli, M. Salanne, and G. W. Watson, Phys. Chem. Chem. Phys. **16**, 8320 (2014).
[23] J. C. Slater and J. G. Kirkwood, Phys. Rev. **37**, 682 (1931).
[24] G. J. Martyna, D. J. Tobias, and M. L. Klein, J. Chem. Phys. **101**, 4177 (1994).
[25] P. P. Ewald, Annalen der Physik **369**, 253 (1921).
[26] E. Rangasamy, J. Wolfenstine, J. Allen, and J. Sakamoto, J. Power Sources **230**, 261 (2013).
[27] K. Meier, T. Laino, and A. Curioni, J. Phys. Chem. C **118**, 6668 (2014).
[28] A. Kuhn, S. Narayanan, L. Spencer, G. Goward, V. Thangadurai, and M. Wilkening, Phys. Rev. B **83**, 094302 (2011).
[29] M. Klenk and W. Lai, Phys. Chem. Chem. Phys. **17**, 8758 (2015).
[30] S. Adams and R. P. Rao, J. Mater. Chem. **22**, 1426 (2011).
[31] L. J. Miara, S. P. Ong, Y. Mo, W. D. Richards, Y. Park, J. M. Lee, H.-S. Lee, and G. Ceder, Chem. Mater.‘ **25**, 3048 (2013).
[32] R. Jalem, Y. Yamamoto, H. Shiiba, M. Nakayama, H. Munakata, T. Kasuga, and K. Kanamura, Chem.

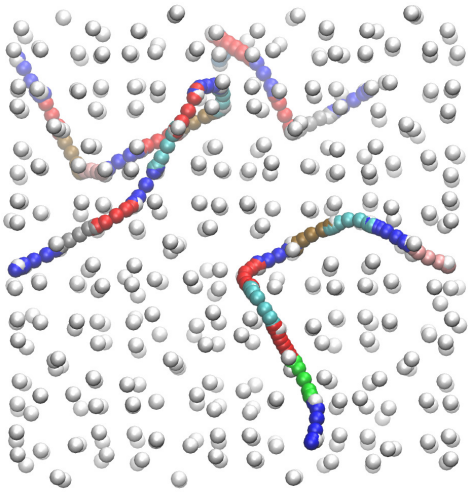

FIG. S4. Schematic of a "coalescent" excitation event observed in t-LLZO at 300 K, highlighting the mobile participating lithium ions.

Mater. **25**, 425 (2013).
[33] G. Larraz, A. Orera, and M. L. Sanjuan, J. Mater. Chem. A **1**, 11419 (2013).
[34] N. Bernstein, M. Johannes, and K. Hoang, Phys. Rev. Lett. **109**, 205702 (2012).
[35] M. Burbano, D. Marrocchelli, and G. Watson, J. Electroceramics **32**, 28 (2013).
[36] A. Kushima and B. Yildiz, J. Mater. Chem. **20**, 4809 (2010).
[37] M. Wilson, P. A. Madden, and B. J. Costa-Cabral, J. Phys. Chem. **100**, 1227 (1996).
[38] A. Aguado and P. A. Madden, Phys. Rev. B **70**, 245103 (2004).